

1 **Partitioning CloudSat Ice Water Content for Comparison with Upper-Tropospheric**
2 **Ice in Global Atmospheric Models**

3

4 Wei-Ting Chen¹, Christopher P. Woods^{1,2}, Jui-Lin Li¹, Duane Waliser¹, Jiun-Dar Chern³,
5 Wei-Kuo Tao³, Jonathan Jiang¹, and Adrian M. Tompkins⁴

6

7 ¹Jet Propulsion Laboratory, California Institute of Technology, Pasadena, California,
8 USA

9 ²Now at The Aerospace Corporation, El Segundo, California, USA

10 ³NASA Goddard Space Flight Center, Greenbelt, Maryland, USA

11 ⁴European Centre for Medium-Range Weather Forecasts, Reading, UK and ICTP, Abdus
12 Salam International Centre for Theoretical Physics, Trieste, Italy

13 **Abstract**

14 CloudSat provides important estimates of vertically resolved ice water content (IWC) on
15 a global scale for evaluating the representation of ice clouds in atmospheric models. By
16 using the ice particle size distribution parameters estimated by the CloudSat retrieval
17 algorithm, the present study partitions CloudSat total IWC into small and large ice
18 hydrometeors. The partitioned CloudSat IWC suggests that the small ice particles
19 contribute to 20-30% of the total IWC in the upper troposphere when a threshold size of
20 100 μm is used. Cloud ice analyses from the European Centre for Medium-Range
21 Weather Forecasts model agree well with the small IWC from CloudSat. The finite-
22 volume multi-scale modeling framework model underestimates total IWC at 147 and 215
23 hPa, while overestimating the fractional contribution from the small ice species. These
24 results, along with sensitivity measures, are discussed in terms of their applications to,
25 and implications for, the evaluation of global atmospheric models.

1. Introduction

The millimeter-wave cloud profiling radar (CPR) onboard CloudSat is capable of providing vertically resolved ice water content (IWC) estimates based on radar reflectivity. These estimates of IWC have proven beneficial in evaluating the representations of ice clouds in global models [e.g., *Marchand et al.*, 2009; *Waliser et al.*, 2009]. Important sampling and sensitivity issues associated with the uses of A-Train IWC data for general circulation model (GCM) comparisons and evaluation have been described in previous investigations [e.g., *Waliser et al.*, 2009; *Li et al.*, 2007]. An issue when performing model-data comparisons of IWC particularly germane to this investigation, is the question of which component(s) of the frozen water mass are represented by retrieval estimates and how they relate to model representations. We note that, while it is understood that all ice particles are falling under the influence of gravity, cloud particles tend to be quasi-suspended or “floating” and will be referred as “cloud ice” to distinguish from truly precipitating particles (i.e. snow and graupel). A method that can categorize the ice mass estimated by CloudSat into portions of “suspended”, small particles (cloud ice) and precipitating, large particles (i.e., snow and graupel) is therefore highly imperative, as such distinction allows one to make more meaningful comparisons and provides new insights to GCMs.

As a step beyond comparing vertically resolved estimates of the total IWC against global models, *Waliser et al.* [2009] filtered out retrievals that were flagged by CloudSat algorithms as either exhibiting surface precipitation or the convective cloud types, both of which would be associated with significant amounts of larger falling hydrometeors. The filtered subset (i.e. non-precipitating and non-convective cases) was used as an initial estimate of the suspended ice particles for the comparison to the cloud ice represented in GCMs. The present study aims to develop and apply a technique to partition CloudSat total IWC based on ice particle size distributions, for estimating the amount of ice water mass from particles smaller and larger than a selected particle size. Section 2 describes the CloudSat IWC data, the methodology for partitioning the ice mass, and the models to be compared with the CloudSat estimates. Using an ice particle size threshold to

distinguish between small ice particles and larger precipitating hydrometeors, the total and partitioned CloudSat IWC are presented and compared with model representations in Section 3. The results are summarized in Section 4 along with a discussion of future applications.

2. Data and Models

2.1. CloudSat total and partitioned IWC

CloudSat is one of the five satellites in the A-Train constellation that makes equatorial passes at approximately 1:30 am and 1:30 pm local time, measuring vertical profiles of radar reflectivity. IWC analyzed in the present study is retrieved from the CloudSat Radar-Visible Optical Depth Cloud Water Content retrieval algorithm (2B-CWC-RVOD, v5.1, R04). This algorithm is a modification of the Radar Only algorithm by *Austin et al.* [2009] (an earlier version is described by *Benedetti et al.* [2003]). The forward model assumptions for ice particle size distribution (PSD) and the uncertainty of the retrievals are described briefly in the Supporting Material I.

The CloudSat total IWC (IWC_{TOTAL}) can be partitioned into portions of particles smaller and larger than a specific cutoff size (D_c). By representing the ice particles as equivalent spheres with diameter D and constant ice density ρ_i , the partitioned IWC of ice particles larger than D_c ($IWC_{>D_c}$) is derived by integrating the third-moment of the lognormal PSD $N(D)$ with D_c as the lower limit,

$$IWC_{>D_c} = \int_{D=D_c}^{D=\infty} \rho_i \frac{\pi}{6} N(D) D^3 dD \quad (1)$$

The partitioned IWC of ice particles smaller than D_c ($IWC_{<D_c}$) is computed by subtracting $IWC_{>D_c}$ from IWC_{TOTAL} . Figure 1a shows a sample lognormal PSD (red line) and its corresponding mass distribution (black line). An example of cutoff size $D_c = 100 \mu\text{m}$ (dotted line) is used to demonstrate the partitioning of $IWC_{<100}$ (green area) and $IWC_{>100}$ (blue area).

83

84 As the retrieval algorithm does make a priori assumptions, the partitioned IWC presented
85 here represents the interpretation specifically based on the RVOD products. The
86 partitioned IWC will be affected by the algorithm employed to retrieval ice PSD
87 parameters (see Supporting Material II), as well as the choice of the cutoff size and the
88 retrieved PSD parameters (Section 3.1). However, we would like to stress that model
89 estimates of ice water path (IWP) vary by two orders of magnitude [Waliser *et al.*, 2009],
90 and thus having a quantitative estimate, such as that described here, has significant value.
91 Moreover, it prototypes a useful technique that can be elaborated on with the
92 development of increasingly sophisticated instruments and algorithms.

93

94 **2.2. Model representations of IWC: ECMWF and fvMMF**

95 Waliser *et al.* [2009] provide an overview of the methodologies used by several GCMs to
96 represent atmospheric ice. Most GCMs use simple ice representations with the
97 consideration of computational efficiency. The GCM parameterizations typically divide
98 the total frozen condensate into an amount that remains “suspended” in the atmosphere
99 and an amount expected to fall as precipitation either instantly onto the surface or with
100 sedimentation considered in one model time step. Given the variety of techniques,
101 significant difficulties exist when attempting to compare CloudSat IWC estimates to
102 modeled IWC, since the CPR detects all frozen particles producing the 94 GHz radar
103 reflectivity echo, and therefore the suspended and falling particles are included in the
104 CloudSat estimates.

105

106 The present study compares the CloudSat IWC with the estimates from the European
107 Centre for Medium-Range Weather Forecasts (ECMWF) Integrated Forecast System
108 (IFS CY31R1). Two kinds of ice crystals are represented in the ECMWF model: “pure
109 ice” and “snow” [Tiedtke, 1993]. In the revised scheme, there is no size threshold
110 separating the two species; an explicit autoconversion term that converts ice to snow and
111 a new scheme for ice crystal sedimentation scheme are applied [Jung *et al.*, 2010]. The

falling/sedimentation rates of condensates are determined by temperature and ice particle size. Immediate fall-out is assumed for snow upon formation, with sublimation and melting in lower levels. The cloud scheme includes processes such as the detrainment of condensates in convection updrafts, collection, accretion, and evaporation. A scheme for homogeneous ice nucleation that allows ice supersaturation to exist in the clear sky is also implemented [Tompkins *et al.*, 2007].

The difficulties that arise for comparing CloudSat ice contents with GCMs with simplified ice microphysics are somewhat mitigated for models with a multispecies microphysics scheme, such as the Goddard finite-volume multi-scale modeling framework (fvMMF; Tao *et al.* [2003]). In such models, both suspended and precipitating forms of ice may coexist at any model grid point without instantaneous fallout. The fvMMF employs a single-moment bulk microphysical scheme with water vapor, cloud water, rain, cloud ice, snow and graupel. Figure 1b shows sample PSDs for snow and graupel that could exist at an fvMMF grid point. Since the modeled ice species each follow defined distributions, the ice mass can be readily partitioned by particle size into a contribution from ‘small’ and ‘large’ ice mass with respect to a specified size cutoff. This, coupled with the PSD partitioning technique developed here, provides a basis for model evaluation of IWC with some level of size distribution consideration, which would otherwise be very difficult to achieve. Note that in the fvMMF ice parameterization, the cloud ice species is represented as a mono-dispersed quantity with a size less than 100 μm . Therefore, all of the mass for cloud ice would be attributed to the “small” size category if the chosen cutoff size is larger than 100 μm .

3. Results

3.1 Monthly Mean CloudSat Partitioned IWC and Sensitivities

While there is no definitive threshold that defines non-precipitating and precipitating ice particles, the threshold D_c for partitioning the CloudSat IWC PSD is set to 100 μm as a simplistic attempt to separate the small, non-precipitating and the large, precipitating ice

particles detected in the upper atmosphere by CloudSat, based on work presented in Ryan [2000]. Sensitivity analysis to the specification of threshold (see the discussion below), the retrieved PSD parameters (see below), and the retrieval products (the Supporting Material II) is presented. In the global maps presented below, the monthly mean IWC fields are spatially averaged into 8° longitude by 4° latitude grids which is compromise between a grid size that is comparable to GCM model output, adequate to capture monthly mean variability, and provide adequate samples for each box given CloudSat's nadir-only sampling.

Fig. 2 shows the monthly average IWC_{TOTAL} , $IWC_{>100}$, and $IWC_{<100}$ retrieved by CloudSat RVOD algorithm in August 2006. Areas with frequent and intense convective activities, such as the Tropical Western Pacific and central Africa, exhibit maximum IWC_{TOTAL} up to 16 mg m^{-3} and 30 mg m^{-3} , respectively, at 147 hPa and 215 hPa. The partitioned IWC estimates from the CloudSat suggest that about 20-30% of IWC_{TOTAL} in the upper troposphere comes from ice particles smaller than $100 \text{ }\mu\text{m}$. Waliser *et al.* [2009] estimated sampled CloudSat IWC for cloud ice by excluding surface precipitation or convective cloud cases. Both the amount and geographical distribution of the smaller ice mass ($IWC_{<100}$) derived in the present study match closely to the filtered CloudSat IWC present in Waliser *et al.* [2009], despite the different methods adopted in the two studies to estimate the cloud ice mass.

The partitioning of IWC in the manner described in this study is not limited to a simple small versus large particle partitioning. Any relevant number of size ranges and thresholds may be applied. The sensitivity of the partitioned IWC to the choice of the cutoff size D_c is demonstrated in Fig. 3. As D_c varies from $75 \text{ }\mu\text{m}$ to $150 \text{ }\mu\text{m}$, the global monthly mean fraction of the small ice species ($IWC_{<D_c}$) at 215 hPa (black solid line) increases from 5% to 35%. At 147 hPa, the fraction of the small ice species is higher (black dotted line), with a similar but stronger sensitivity (i.e. steeper slope) to the values of D_c .

As the IWC partitioning is based on the retrieved PSD, uncertainties in the PSD parameters would lead to uncertainties in the partitioned ice mass. A second sensitivity is carried out to provide a basic estimation of this uncertainty propagation. In the 2B-CWC-RVOD algorithm (see Supporting Material I), *a priori* values of the geometric mean diameter (D_g) and the width parameter (σ_{lo}) are empirical functions of temperature (from ECMWF analysis), while the *a priori* total number concentration (N_T) is determined by both the reflectivity (through the Z_e -IWC relationship) and temperature (through the IWC-PSD relationships with *a priori* D_g and σ_{lo}). The sensitivity test is constructed by following a procedure analogous to the retrieval algorithm. For all CloudSat IWC retrievals, both the D_g and σ_{lo} are perturbed by 20% of their retrieved values. The corresponding change in N_T is calculated, retaining IWC_{TOTAL} at the retrieved value. The perturbed $IWC_{>DC}$ is then derived from equation 1 using the perturbed PSD parameters. Note that increasing (decreasing) either D_g or σ_{lo} would flatten (narrow) the PSD and shift the peak of the distribution towards larger (smaller) sizes, leading to an increase (decrease) in the mass fraction of large ice particles. Therefore varying both parameters simultaneously in the same direction represents the extreme cases of the PSD shape biases. The error bars in Fig. 3 show the sensitivity of the global monthly mean IWC fractions to a 20% perturbation of both D_g and σ_{lo} . For the case of $D_c=100\text{ }\mu\text{m}$, the mean mass fraction of small ice particles is changed from 11% to as much as 36%. The sensitivity is higher for larger cut off sizes, and is similar between the 215 hPa and 147 hPa levels.

3.2 CloudSat and Model Comparisons

Fig. 4a shows the monthly mean IWC from the ECMWF IFS CY31R1 in August 2006. At the upper-tropospheric levels considered (147 hPa and 215 hPa), ice mass represented in the ECMWF model are mostly from cloud ice. At both levels monthly averaged ECMWF total IWC and the CloudSat $IWC_{<100}$ (Fig. 2c) agree to within 10%. Similar results were found for January 2007 (not shown). Waliser *et al.* [2009] also identified good agreement between the IWC from the ECMWF CY31R1 analysis and the subset of CloudSat IWC from non-precipitating and non-convective cases.

The partitioned CloudSat IWC estimates were used to assess fvMMF model output (Fig. 4b-d). Total IWC from the fvMMF model is partitioned into “small” and “large” categories using the same 100 μm threshold as in Section 3.1. IWC_{TOTAL} from the fvMMF (Fig 4b) are underestimated at both 147 hPa and 215 hPa when compared to CloudSat estimates (Fig. 2a). As revealed by the zonal mean IWC vertical profiles in *Waliser et al.* [2009], the altitude of maximum total IWC over the Tropics predicted in the fvMMF is lower (at 500-600 hPa) than the CloudSat estimates (at 250-400 hPa), while the IWP is well simulated by the model. Therefore the total IWC in fvMMF is generally underestimated above 400-450 hPa, and overestimated below these altitudes.

Figs. 4c and 4d show that the modeled IWC field is nearly an even split ($\sim 50\%$) between the small ($IWC_{<100}$) and large ($IWC_{>100}$) ice particles in the upper troposphere. The partitioned CloudSat estimates (Figs. 2b, c) suggest that, for a cutoff size of 100 μm , about 20-30% of the total IWC is comprised of the small, non-precipitating ice particles. The comparison indicates that the fvMMF may overestimate the mass of cloud ice and underestimate the mass of large, precipitating ice particles at the levels considered. These findings are consistent with those in *Marchand et al.* [2009] that excessive hydrometeor coverage exists in the fvMMF at upper troposphere during northern summer in the western Pacific. The differences between model and retrieved estimates are likely related to the deposition velocity assumed in the model for large ice particles.

4. Summary

The vertically resolved IWC estimates from CloudSat provide crucial observational constraints that can be applied to evaluate the representations of ice clouds in global models. The present study uses retrieved ice particle size distribution parameters from CloudSat 2B-CWC-RVOD algorithm to partition atmospheric ice mass. This technique guarantees relevant comparisons of CloudSat IWC estimates against global models.

Applying an ice particle size threshold of 100 μm to separate the contributions of the small and large ice particles, the partitioned IWC values indicate that 20-30% of the total ice mass estimated by CloudSat is from small ice particles ($< 100 \mu\text{m}$). Comparisons of monthly averaged partitioned CloudSat $IWC_{<100}$ to the ECMWF cloud ice analyses showed a close agreement at 147 hPa and 215 hPa. IWC model output from the fvMMF were partitioned by size in the same fashion as the CloudSat IWC estimates. The comparisons reveal that the fvMMF underestimates IWC in the upper troposphere at the altitudes considered, and overestimates the fractional contribution from the small particle to the total ice mass (50%, while the CloudSat estimates suggest 20-30%).

The current results can be used in future study to compare CloudSat IWC to other remotely sensed estimates (e.g., Microwave Limb Sounder). A similar assessment will also be performed for CloudSat retrieved liquid water content. The values generated by the partitioning technique can be applied for level-by-level comparisons of cloud ice or liquid. Further study is also permitted using the partitioning technique by integrating mass contents over more refined bin sizes to better identify potential model parameterization improvements.

Acknowledgments

CloudSat data were provided by NASA CloudSat project through Colorado State University. This research was carried out at the Jet Propulsion Laboratory, California Institute of Technology, under a contract with NASA. It is supported by NASA CloudSat program.

References

- Austin, R. T., A. J. Heymsfield, and G. L. Stephens (2008), Retrievals of ice cloud microphysical parameters using the CloudSat millimeter-wave radar and temperature. *J. Geophys. Res.*, submitted.
- Chen, J.-P., G. M. McFarquhar, A. J. Heymsfield, and V. Ramanathan (1997), A

259 modeling and observational study of the detailed microphysical structure of tropical
 260 cirrus anvils, *J. Geophys. Res.*, 102, 6637-6653.

261 Heymsfield, A. J, et al. (2008), Testing IWC Retrieval Methods Using Radar and
 262 Ancillary Measurements with In Situ Data, *J. Appl. Meteorol. Clim.*, 47, 135–163,
 263 doi10.1175/2007JAMC1606.1.

264 Jung, T., et al. (2010), The ECMWF model climate: Recent progress through improved
 265 physical parametrizations, *Q. J. Roy. Meteorol. Soc.*, in press.

266 Li, J. L., J. H. Jiang, D. E. Waliser, and A. M. Tompkins (2007), Assessing consistency
 267 between EOS MLS and ECMWF analyzed and forecast estimates of cloud ice,
 268 *Geophys. Res. Lett.*, 34, L08701, doi:10.1029/2006GL029022.

269 Marchand, R., J. Haynes, G. G. Mace, T. Ackerman, and G. Stephens (2009), A
 270 comparison of simulated cloud radar output from the multiscale modeling
 271 framework global climate model with CloudSat cloud radar observations, *J.*
 272 *Geophys. Res.*, 114, D00A20. doi:10.1029/2008JD009790.

273 McFarquhar, G. M., and A. J. Heymsfield (1998), The Definition and Significance of an
 274 Effective Radius for Ice Clouds. *J. Atmos. Sci.*, 55, 2039–2052.

275 Ryan, B. F. (2000), A Bulk Parameterization of the Ice Particle Size Distribution and the
 276 Optical Properties in Ice Clouds. *J. Atmos. Sci.*, 57, 1436–1451.

277 Tao, W. K., et al. (2003), Microphysics, radiation and surface processes in the Goddard
 278 Cumulus Ensemble (GCE) model, *Meteorology And Atmospheric Physics*, 82(1-4),
 279 97-137.

280 Tiedtke, M., (1993), Representation of clouds in large-scale models. *Mon. Weather Rev.*,
 281 121, 3040-3061.

282 Tompkins, A. M., Gierens, K., and Rädcl, G. (2007), Ice supersaturation in the ECMWF
 283 Integrated Forecast System, *Q. J. Roy. Meteorol. Soc.*, 133, 53–63.

284 Waliser, D. E., et al. (2009), Cloud ice: A climate model challenge with signs and
 285 expectations of progress. *J. Geophys. Res.*, 114, D00A21,
 286 doi:10.1029/2008JD010015.

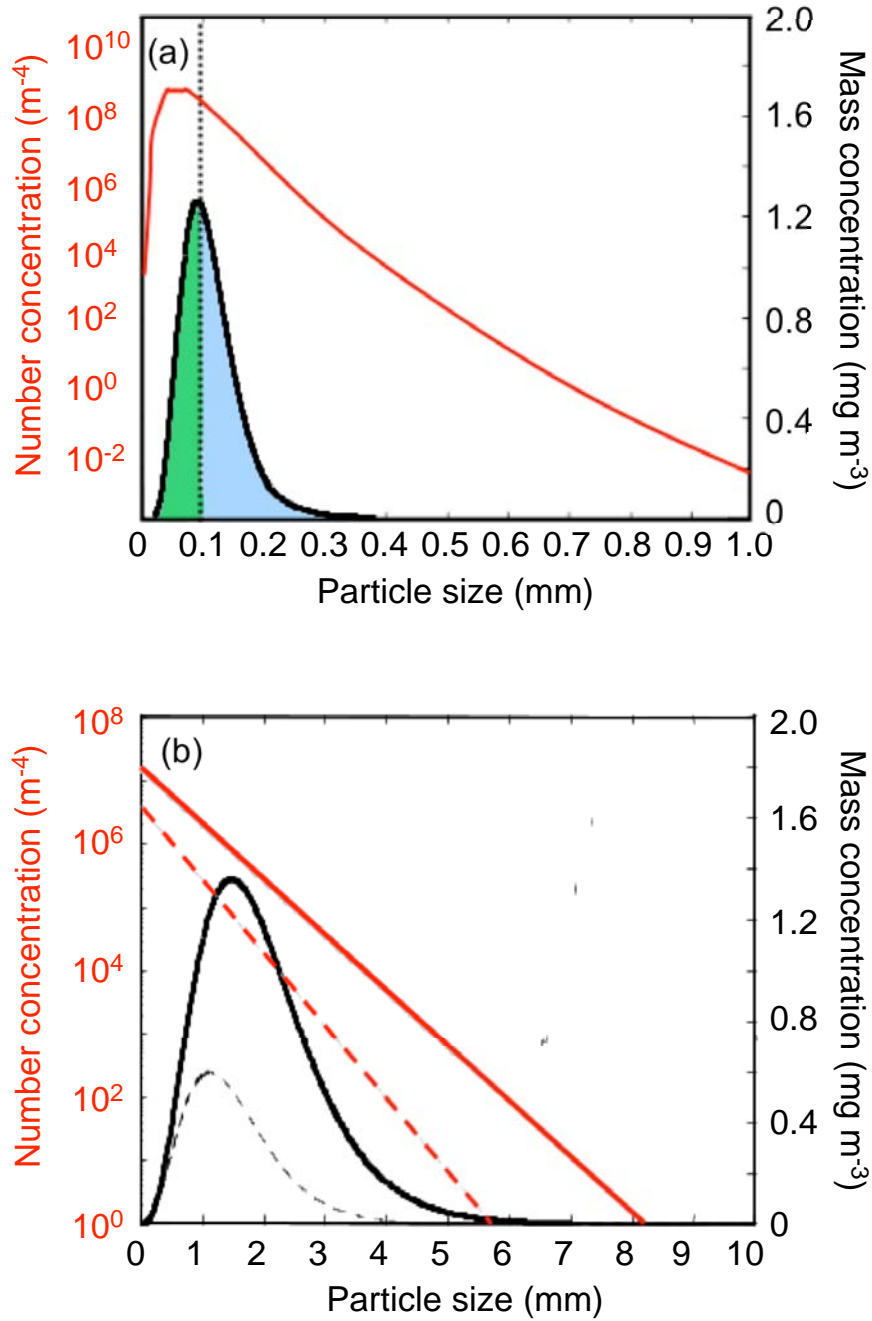


Figure 1. (a) A sample lognormal ice number distribution (red curve; left ordinate), and the corresponding mass distribution (black curve; right ordinate). The dotted line represents the cutoff size for IWC partitioning ($D_c = 100 \mu\text{m}$ as an example). The partial integrals of the mass distribution for particles smaller and larger than D_c correspond to $IWC_{<100}$ (green area) and $IWC_{>100}$ (blue area), respectively. (b) Sample lognormal number distributions (red curves; left ordinate) and exponential mass distributions (black curves; right ordinate) for snow (solid lines) and graupel (dashed lines) used in the fvMMF. The total mass concentration for snow and graupel is 0.30 gm^{-3} and 0.10 gm^{-3} , respectively.

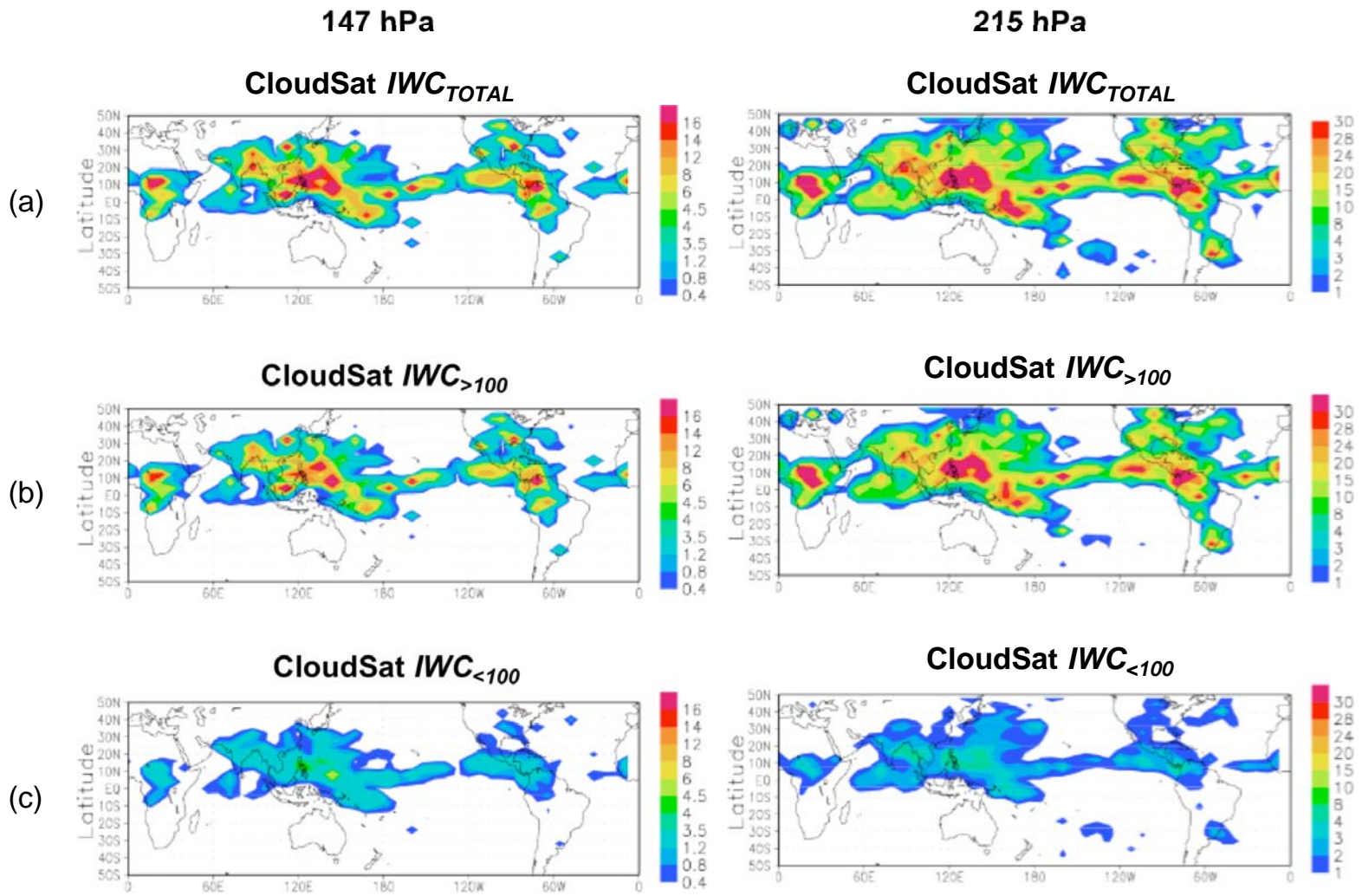


Figure 2. Monthly average values of (a) IWC_{TOTAL} , (b) $IWC_{>100}$, and (c) $IWC_{<100}$ from CloudSat RVOD retrievals in August 2006 (in mg m^{-3}), plotted at a $8^\circ \times 4^\circ$ resolution. The values at 147 hPa (left) and 215 hPa (right) are shown.

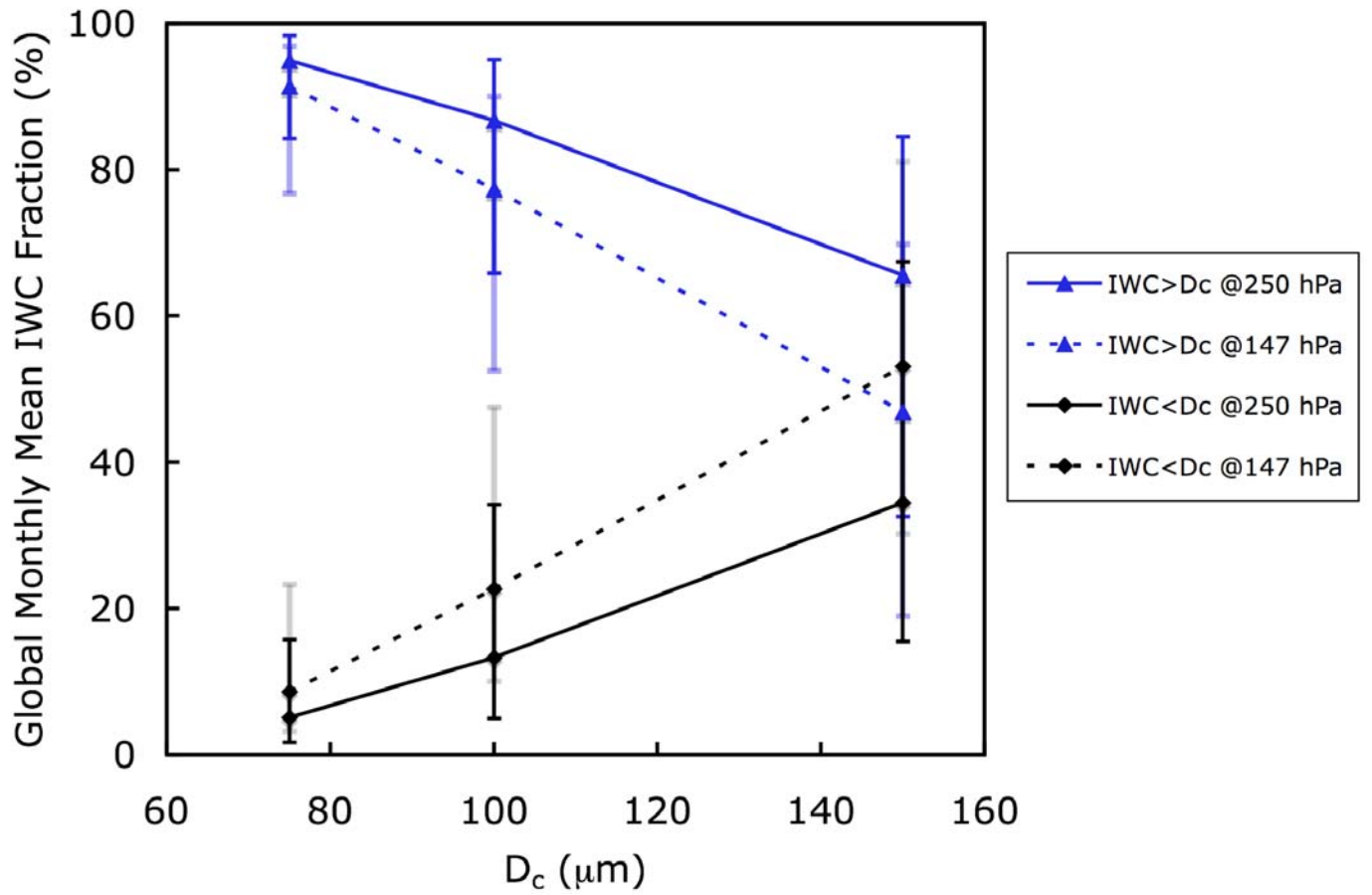
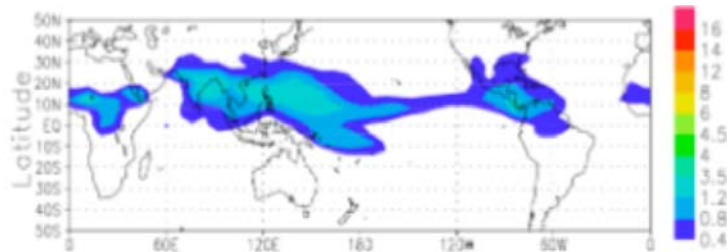


Figure 3. Global monthly mean fractions of partitioned IWC (in %) as a function of the cutoff size (D_c). $IWC_{<D_c}$ (black lines) and $IWC_{>D_c}$ (blue lines) at 215hPa (solid lines) and 147hPa (dotted lines) from CloudSat RVOD products in August 2006 are shown. The error bars represent the results of perturbing the retrieved size distribution parameters by 20% with the assumption of conserving IWC. Details are provided in Section 3.1.

147 hPa

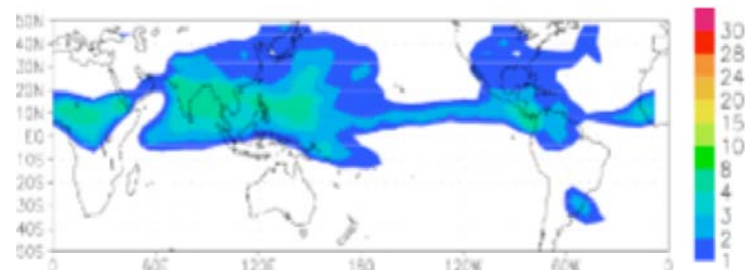
ECMWF CY31r1

(a)

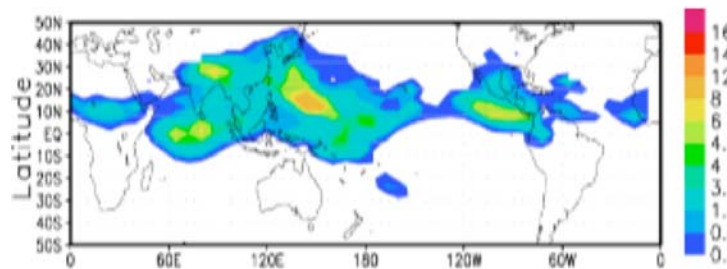
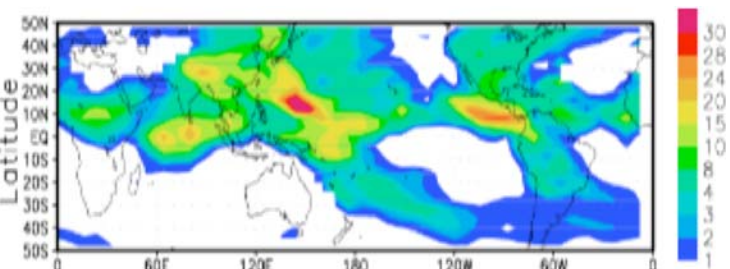


215 hPa

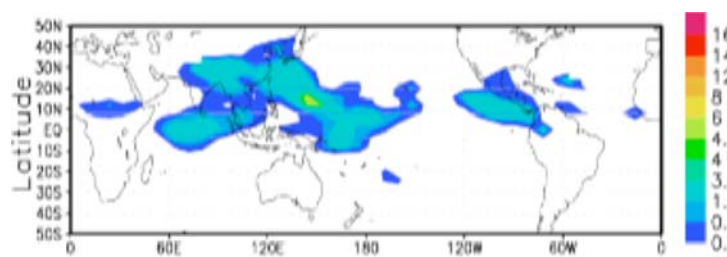
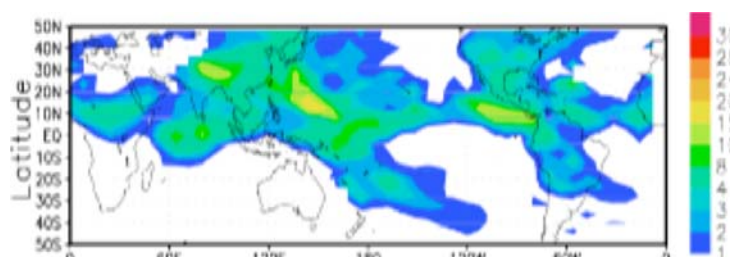
ECMWF CY31r1

fvMMF IWC_{TOTAL}

(b)

fvMMF IWC_{TOTAL} fvMMF $IWC_{>100}$

(c)

fvMMF $IWC_{>100}$ fvMMF $IWC_{<100}$

(d)

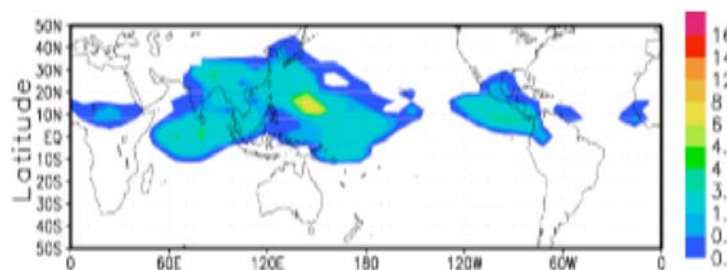
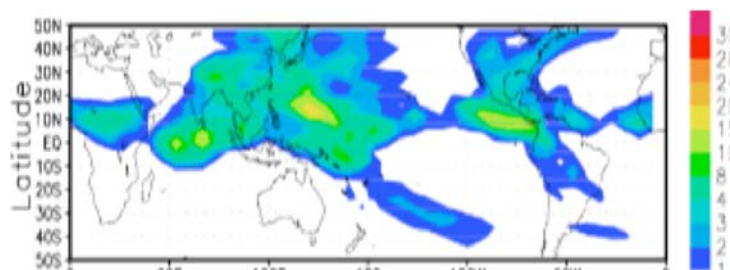
fvMMF $IWC_{<100}$ 

Figure 4. Monthly mean (a) total IWC from ECMWF IFS, and (b) IWC_{TOTAL} , (c) $IWC_{>100}$, and (d) $IWC_{<100}$ from the fvMMF for August 2006 (in mg m^{-3}), plotted at a $8^\circ \times 4^\circ$ resolution. The values at 147 hPa (left) and 215 hPa (right) are shown.